Influence of Mg Concentration on the Inhibiting Effect of CO_2 on the Rate of Oxidation of Aluminum Alloys 5182 and 6016

Cathrine Kyung Won Solem, Egil Solberg, Gabriella Tranell, and Ragnhild E. Aune

Abstract

Oxidation of aluminum alloys during production is a well-known problem and contributes to significant metal losses. As small additions of CO_2 in the oxidizing atmosphere has proven to inhibit the oxidation rate for high-Mg($\geq$5wt%) aluminum alloys, the present study has aimed at evaluating its effect on alloys with varying Mg concentration in combination with other alloying elements (Si and Mn), i.e. Al alloys 5182 (AlMg4.6Mn0.4) and 6016 (AlSi1.2Mg0.4). Experiments were performed by DSC-TG (Differential Scanning Calorimetry–Thermogravimetric Analysis) using three different cover gases, i.e. (i) 80% *synthetic air* and 20% argon, (ii) 99.999% *argon,* and (iii) *4% CO_2*, 20% argon and 76% synthetic air while monitoring the mass change and heat flux at 750 °C for 7 h. A significant inhibiting effect was observed for alloy 5182 during exposure to *CO_2*, with a mass loss of -0.3%, when compared to the results obtained for *synthetic air* and *argon* having mass gains of 11.21% and 1.67%, respectively. The thickness of the oxide layer was also influenced and decreased stepwise from *synthetic air*, to *argon* and *CO_2*. A similar effect was observed to a lesser extent for alloy 6016 due to the lower Mg concentration, decreasing the mass gain from 2.45% when heated in *synthetic air* to 1.61% in *argon* and 0.7% in *CO_2*. The thickness of the oxide layer decreased in *argon* and increased to almost similar thicknesses in *synthetic air* and *CO_2*. The lower mass gain in *CO_2* proves that CO_2 has an inhibiting effect on the oxidation rate even for low-Mg alloys.

C. K. W. Solem (✉) · G. Tranell · R. E. Aune
Dept. of Materials Science and Engineering, Norwegian University of Science and Technology (NTNU), Trondheim, Norway
e-mail: cathrine.k.w.solem@ntnu.no

E. Solberg
Alcoa Norway ANS, Mosjøen, Norway

Keywords

Aluminum • Oxidation • TGA • DSC • Synthetic air • Argon • CO_2

Introduction

Oxidation of aluminum (Al) and its alloys is a well-known problem, generating an aluminum dross. The aluminum dross typically contains up to 70% metallic Al, causing severe losses up to 10% metallic Al [1]. To prevent and reduce these losses, several studies have over the years been performed by different research groups with the aim to inhibit the oxidation rate of Al alloys [2–5].

Behavior of Mg at Elevated Temperatures

The aluminum–magnesium (AlMg) system has been given special attention, as the Mg concentration has proven to influence the rate of oxidation of Al alloys [6–8]. As early as in 1961, Cochran and Sleppy [7] reported a significantly higher mass gain for an AlMg alloy with 2.35 wt% Mg compared to high-purity Al, and their results were later confirmed by other studies [9–11].

Mg is frequently used in Al alloys to maintain the already low weight of Al, which is attractive to the transportation and packaging industry. During the production of Al alloys with Mg as one of the most important alloying elements, challenges during the processing of the liquid melt may occur due to its high affinity to oxygen [12]. Significant fractions of the added Mg are lost due to oxidation and evaporation, as the melt is often processed at elevated temperatures, e.g. 750 °C, causing generation of oxides, e.g. MgO (magnesium oxide) and $MgAl_2O_4$ (spinel, magnesium aluminum oxide) [13, 14]. Formation of oxides was revealed by monitoring the mass gain, as the oxides, i.e. MgO (ρ_{MgO}

© The Minerals, Metals & Materials Society 2021

L. Perander (ed.), *Light Metals 2021*, The Minerals, Metals & Materials Series,
https://doi.org/10.1007/978-3-030-65396-5_97

$_{(liq)}$ = 3.58 g/cm^3) and $MgAl_2O_4$ ($\rho_{MgAl2O4(liq)}$ = 3.58 g/cm$_3$) have higher densities than both Mg ($\rho_{Mg(liq)}$ = 1.6 g/cm$_3$) and Al ($\rho_{Al(liq)}$ = 2.4 g/cm^3) [15]. However, evaporation of Mg has been demonstrated to be hindered when adding small amounts of CO_2 in the atmosphere, inhibiting the oxidation rate of the alloy [14].

The $AlMgSiO_2$ Systems

A body of work exists for the AlMg system, and an extension of the system, adding a third element, i.e. Si, has also been performed to investigate the influence on the oxidation rate [12]. In an earlier study by some of the current authors, it was reported that the AlMgSi alloy having >6 wt% Mg and >6 wt% Si oxidized rapidly in synthetic air, while a reduction in the oxidation rate was observed in an inert cover gas, i.e. in Ar [12]. When adding $\geq$5 wt% CO_2 to the atmosphere, an inhibiting effect was identified, decreasing the mass gain and the oxide layer thickness [12]. The oxide layer morphology and chemical composition had similar features as the oxides formed on an AlMg alloy, where the oxidation had been limited by CO_2 being absorbed onto the initial MgO layer, hindering further evaporation and oxidation of the alloy [12, 14]. MgO and $MgAl_2O_4$ were revealed to be the main compounds in the oxide layers. Some Mg_2Si (s) (magnesium silicide) was found to form where the activity of Al was sufficiently low [12].

The $AlMgMnO_2$ System

The AlMn alloy system is frequently used as the Mn contributes to a hardening of the alloy, making it suitable for several applications, e.g. cans and pipes. The amount of Mn added does usually not exceed 1.5 wt% as the alloy becomes too fragile, and fractures will easily arise. To increase the hardening of the alloy even more, the AlMn is alloyed with Mg. The stability diagrams for the $AlMgMnO_2$ system as a function of the O_2 (g) partial pressure and the activity of Mg (liq) and Al (liq) can be seen in Fig. 1a and b, respectively. As can be seen in Fig. 1a MgO will co-exist with AlMn, and from Fig. 1b that with an increase in the partial pressure of O_2 a phase transition of MgO to SPIN ($MgAl_2O_4$) together with AlMn-containing phases will occur at higher activities of Al (liq).

There is still a lack of knowledge in regard to the inhibiting effect obtained having small amounts of CO_2 in the atmosphere for low-Mg Al alloys containing even other alloying elements such as Si and Mn.

Experimental Procedure

In the present study, the influence of alloy composition and the inhibiting effect of CO_2 on the oxidation rate of Al alloys 5182 and 6016 (provided by Alcoa Norway ANS), i.e. AlMg4.5Mn0.35 and AlSi1.2Mg0.35, respectively, have been investigated. The samples were cut, sanded to 5 µm grid, and stored in ethanol following the same procedure as earlier reported by Solem et al. [12]

Monitoring of Mass Gain

A NETZSCH Simultaneous Thermogravimetric Analyzer (STA) model Jupiter 449 F (a DSC-TG unit) was applied to monitor the mass change and heat flux as a function of time and temperature. The polished disc samples were removed from the container with ethanol and dried in air for 30 s before heated from 25 to 750 °C with a heating rate of 10 °C/min, followed by an isothermal segment at 750 °C for 7 h, and cooled to 25 °C at the same rate (10 °C/min). Three parallels were run for each Al alloy in three different cover gases, i.e. (i) 80% *synthetic air* (20% O_2 and 80% N_2) and 20% argon, (ii) 99.999% *argon,* and (iii) 76% synthetic air (20% O_2 and 80% N_2), 20% Ar, and 4% *CO_2* (from here on referred to as *synthetic air*, *argon,* and *CO_2*, respectively).

Surface Morphology and Elemental Mapping of Cross Section

The heat-treated disc samples from the DSC-TG experiments were further analyzed in microscope. A Zeiss Ultra model 55LE Scanning Electron Microscopy (SEM) was applied to investigate the surface morphology of the disc samples. Subsequently, the samples were mounted in epoxy, cut, and sanded to evaluate the cross sections, i.e. the oxide layer, as well as the bulk alloy. A JEOL JXA-6500F Field Emission Electron Probe Microanalyzer (EPMA) was later used to conduct elemental mapping of the cross sections, and a Zeiss Supra model 55VP SEM to perform Energy-Dispersive Spectroscopy (EDS) line scans through the oxide layer from the surface into the bulk.

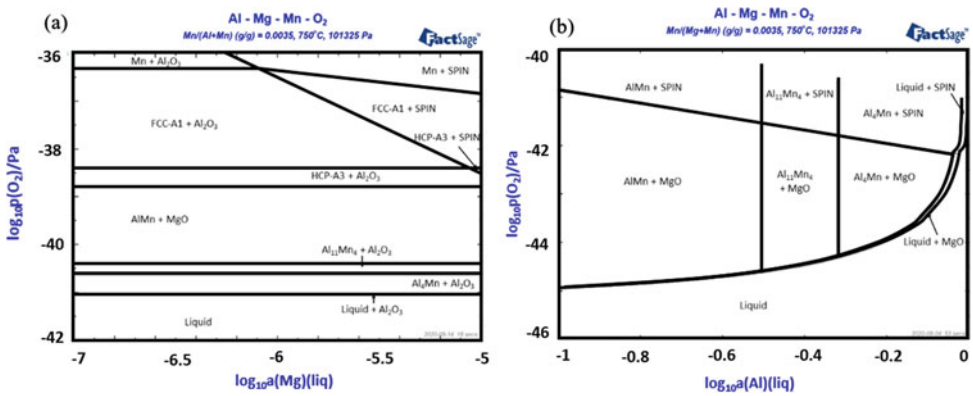

Fig. 1 Al–Mg–Mn–O_2 stability diagrams calculated as a function of the partial pressure of O_2 and the activity of **a** Mg(liq) and **b** Al(liq), respectively. Calculations were performed by the use of the FactSage 7.1 software [15]

Results

Surface Morphology

The heat-treated aluminum disc samples investigated by SEM at a magnification of 5000X showed a clear difference in surface morphologies for different alloys and cover gases, see Fig. 2. From Fig. 2a–c, it is seen, as previously reported [12], that the Al alloy 5182 revealed a granular cauliflower-shaped morphology when exposed to *synthetic air*, a finer cubic-shaped structure when exposed to *argon*, and a horizontal structure/texture when exposed to CO_2.

For the Al alloy 6016, a cauliflower-shaped surface morphology was obtained for the chosen magnification of 5000X for all three cover gases, see Fig. 2d–f.

Mass Gain (TG)

When looking at the thermogravimetric (TG) analyses from the DSC-TG experiments, seen in Fig. 3, both alloys revealed the highest mass gain when exposed to *synthetic air*. The Al alloy 5182 presented in Fig. 3a had an average mass gain (over the three parallels) of 11.21% (dotted light gray graph), 1.67% (dashed dark gray graph) and −0.30% (straight black graph) when exposed to *synthetic air*, *argon* and CO_2, respectively. The same trend in regards to a decreasing mass gain was observed for the Al alloy 6016 as well, having a mass gain in *synthetic air* of 2.45% (dotted light gray graph), in *argon* 1.61% (dashed dark gray graph), and in CO_2 0.7% (straight black graph), see Fig. 3b.

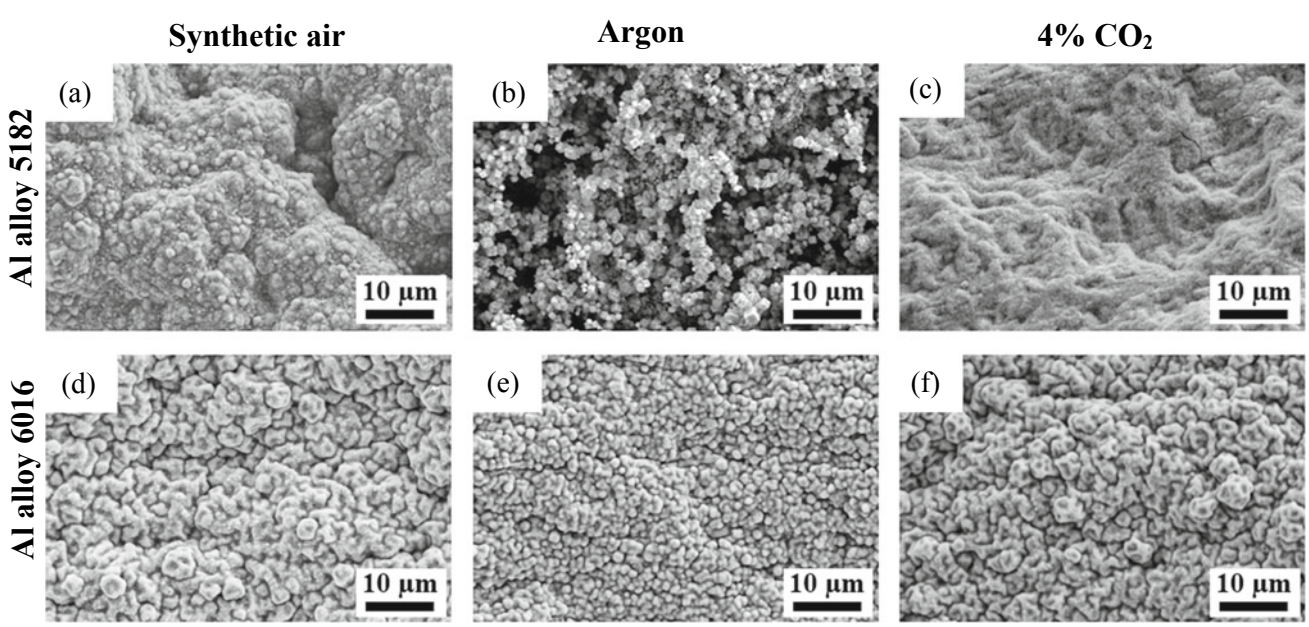

Fig. 2 Scanning Electron Microscopy (SEM) images (Mag = 5000X) of the Al alloy 5182 showing the surface morphology after heat treated at 750 °C for 7 h exposed to **a** synthetic air, **b** argon, and **c** CO_2, showing a clear difference in the surface morphology; and the heated Al alloy 6016 in **d** synthetic air, **e** argon, and **f** CO_2

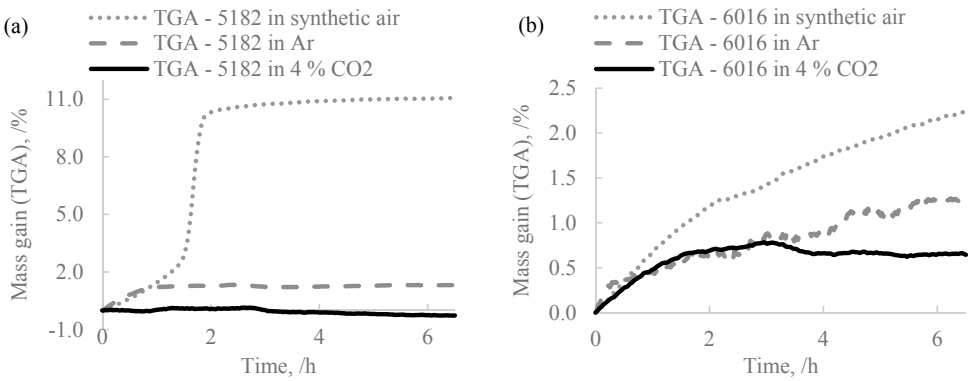

Fig. 3 The mass gain results from the DSC-TG (Differential Scanning Calorimetry–Thermogravimetric Analysis) experiments where disc samples were heated at 750 °C for 7 h in synthetic air (dotted gray graphs), Ar (dashed darker gray graphs) and 4% CO_2 (black straight graphs) for **a** Al alloy 5182 and **b** Al Alloy 6016

Cross-Sectional Evaluation

Figure 4 presents SEM images of the cross section of the resulting oxide layer in the case of heated disc samples of Al alloys 5182 and 6016 taken at a magnification of 400X. The thickness of the oxide layer in regards to the Al alloy 5182 disc samples decreased from 15–27 µm, to 14–17 µm, and 200–400 nm when the cover gas was changed from *synthetic air* to *argon* and later CO_2, see Fig. 4a–c, respectively. Phases within the bulk alloy having higher concentrations of heavier elements, e.g. Mn, were also detected. The thickness of the oxide layer in the case of the low-Mg Al alloy 6016 disc samples was determined to be 4–7 µm when exposed in *synthetic air*, ~1–2 µm in *argon,* and 3–5 µm in CO_2, respectively, see Fig. 4d–f.

Disc samples of both alloys heated in the three different cover gases were mapped by EDS from the surface through the oxide layer and into the bulk material, see Fig. 5. The line scans revealed the presence of four main elements in all samples, i.e. Al (straight white graph), O (dotted light gray graph), Mg (dashed light/dark graph), and C (long-dashed black/dark gray graph). The dashed white lines in the figure (black in Fig. 5a) have diamond ends which mark out where the line scans through the oxide layer were carried out. The general trend is that the concentration of Al decreases when the O and Mg concentrations increase. A rapid decrease

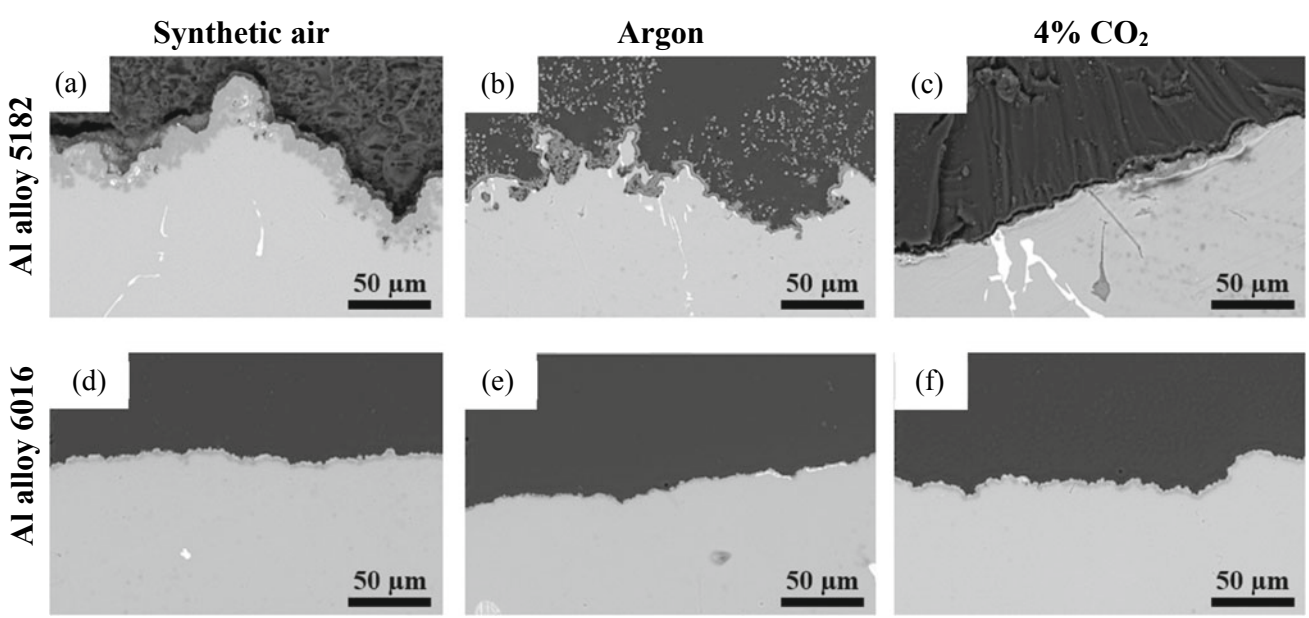

Fig. 4 SEM images (Mag = 400X) showing the oxide layer thickness (cross section) after heat treated at 750 °C for 7 h of of Al alloy 5182 in **a** synthetic air, **b** Ar, and **c** CO_2, and Al alloy 6016 in **d** synthetic air, **e** Ar, and **f** CO_2. The dark gray area is epoxy, the light area is the bulk alloy, and the interface in between is the oxide layer

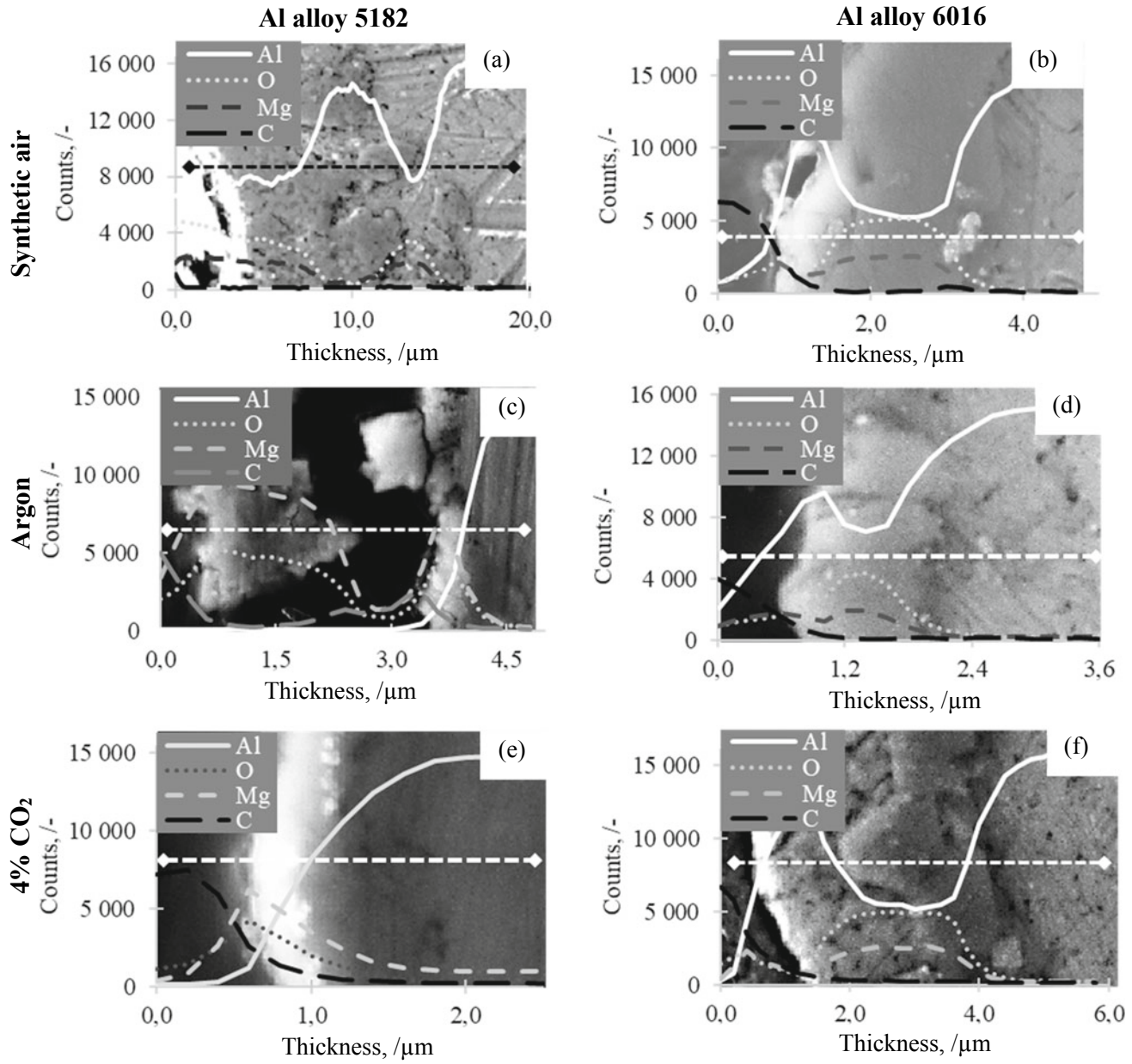

Fig. 5 Energy Dispersive Spectroscopy (EDS) line scans of the cross sections (dashed line with diamond edges) of disc samples heated at 750 °C for 7 h in **a** synthetic air (Al alloy 5182), **b** synthetic air (Al alloy 6016), **c** Ar (Al alloy 5182), **d** Ar (Al alloy 6016), **e** synthetic air and 4% CO_2 (Al alloy 5182), and **f** synthetic air and 4% CO_2 (Al alloy 6016)

from the surface through the oxide layer is also observed for C. No other elements were identified.

Each of the cross sections presented in Fig. 4 was further analyzed by EPMA. The elemental mapping of the areas presented in Fig. 4c and f can be seen in Fig. 6a and b, respectively, where special attention should be given to the differences in the scale bars for each element. The high-Mg containing Al alloy 5182 showed a homogeneous distribution of Al in the bulk metal except for in one area where no Mg and O, where found and at the sample surface where the concentrations of Mg and O again were detected. Mn was mapped to be in the bulk metal together with higher concentrations of Al, Si, and Fe (some of the elemental mappings are presented in Fig. 6a). The low-Mg containing Al alloy 6016 showed a lower concentration of Al at the sample surface together with higher concentrations of Mg and O. The Si was mapped to be homogeneously distributed in the bulk together with the Al, except for in a concentrated area at the sample surface where the Si concentration was significantly higher, see Fig. 6b.

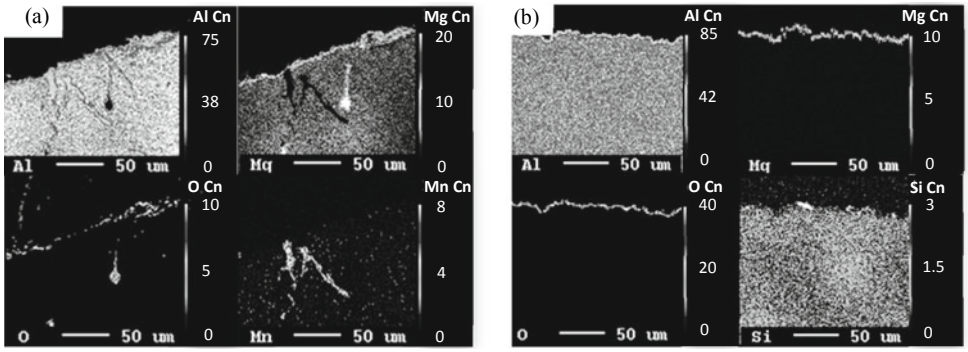

Fig. 6 Electron Probe Micro Analyses (EPMA) of the cross sections presented in Fig. 4c and f after being heat treated at 750 °C for 7 h in 4% CO_2. **a** elemental mapping of Al, Mg, O, and Mn in the case of the Al alloy 5182, where the Mn-rich phase also contains Fe and Si and **b** Al, Mg, O, and Si in the case of Al alloy 6016

Discussion

The Al Alloy 5182

The surface morphologies revealed in SEM for the Al alloy 5182 proved to be similar to what has been reported in literature for high-Mg containing Al alloys [12], i.e. a cauliflower-shaped structure, finer cubes, and a horizontal texture for the disc samples exposed in *synthetic air*, *argon*, and CO_2, respectively, as presented in Fig. 2a–c. This implies that the concentration of Mg had a stronger influence on the overall structure than the absence of Si and/or Mn in the alloy. Another similarity was found in the mass gain, as an inhibiting effect was observed for *argon* and even a greater effect for CO_2, see Fig. 3a. The same observation was also confirmed when the cross sections were investigated, as the thickness of the oxide layer decreased from 15–27 µm to 14–17 µm and to 200–400 nm when changing the cover gas from *synthetic air* to *argon* and CO_2, respectively, see Fig. 4a–c. The EDS line scan for the Al alloy 5182 confirmed the same decrease in the thickness of the oxide layer, as well as a decrease in the Al concentration through the oxide layer when the Mg and O concentrations increased for all three cover gases, however, differences in the concentrations of each of the elements presented in the mapping were found for all the three cover gases.

When exposed to *synthetic air*, the combination of Al, Mg, and O present in the oxide layer has earlier been reported as a two-step breakaway oxidation. This phenomenon could not be confirmed in the case of the disc samples exposed to *synthetic air*, however, a big one-step mass gain was revealed, see gray dotted graph in Fig. 3a. Due to the presence of Al, as can be seen in Fig. 5a, it is believed that the formation of MgO to $MgAl_2O_4$ has occurred as a result of the breakaway oxidation, resulting in one significant mass gain step of 11.21%. This assumption is strengthened even further when looking at the stability diagram of the system Al–Mg–Mn–O_2 presented in Fig. 1b, where the stable phase together with the liquid phase reacts from MgO to SPIN ($MgAl_2O_4$) when the partial pressure of O_2 increases. It is, however, not believed that the phases Al_4Mn, $Al_{11}Mn_4$, or AlMn are present, as no Mn was detected through the oxide layer by EPMA nor found by EDS.

When the Al alloy 5182 was heated in *argon*, the EDS line scan and element mapping revealed nearly no Al present in the granular oxide layer, presented as one big particle in Fig. 5c. The line scan indicated that there was only MgO present in the granular and dense oxide layers. The EPMA results supported these observations. Further oxidation from MgO to $MgAl_2O_4$ has therefore seemingly not taken place. This is confirmed by the dashed dark gray TG curve in Fig. 3a, where *argon* seems to have had a limiting effect on the mass gain, i.e. on the oxidation rate compared with *synthetic air*, lowering the mass gain to 1.61%.

The EDS line scan for the heated disc samples of the Al alloy 5182 in CO_2 revealed a rapid increase of Mg and O in the oxide layer, which linearly decreased as a function of depth into the sample. The concentration of Al increased slowly at first as the Mg and O concentrations increased quickly, followed by a rapid increase as a result of a decrease in the Mg and O concentration. The trends of Mg, O, and Al is confirmed by the EPMA results, where the oxide layer is depleted in Al and concentrated in Mg (continuous layer) and O (discontinuous layer), see Fig. 6a. It was also revealed by the EPMA results that the bulk had a homogeneous distribution of Mg, as well as mapping a concentrated Mg layer at the surface, revealing that the diffusion and evaporation of Mg must have been hindered, see Fig. 6a. From the TG results in Fig. 3a it is clear that small

additions of CO_2 in the cover gas has had a significant inhibiting effect, however, some of the Mg has evaporated from the surface as the average mass gain was found to be negative, i.e. a mass loss of 0.30%.

The Al Alloy 6016

The low-Mg containing Al alloy 6016 did not seem to be as affected by the different cover gases in regard to changes in the surface morphology as the high-Mg containing Al alloy 5182. The morphology of the heated disc samples revealed a cauliflower-shaped structure regardless of the cover gas, see Fig. 2d–f, respectively. Limited differences between the heated disc samples were again recognized when looking at the cross sections, revealing thicknesses of the oxide layers of 4–7, ~1–2, and 3–5 µm for *synthetic air*, *argon*, and CO_2, respectively, as presented in Fig. 4d–f. Key differences were first observed when looking closer at the TG results in Fig. 3b.

It was clear that this alloy had only oxidized to some extent during exposure to *synthetic air* (Fig. 3b, dotted gray graph), revealing a mass gain of 2.45%, explaining why the thickness of the oxide layer was identified to be only 4–7 µm. The EDS line scan in Fig. 5b revealed a higher concentration of Al at the surface, which decreased as the concentrations of O and Mg increased. When reaching the bulk metal, the Al concentration increased again, while the O and Mg concentrations decreased. The presence of Al and MgO at the surface of the disc samples are under the present conditions consistent with the observations made from the stability diagram of Al–Mg–O_2–Si [12]. When the partial pressure of O_2 increases in the oxide layer, as seen in Fig. 5b dashed gray graph, the MgO reacts to form $MgAl_2O_4$. Finally, when reaching the bulk, the concentrations of O and Mg decrease again. No Si was detected by the EDS line scan through the oxide layer, which later were confirmed by EPMA, showing a depletion of Si at the metal surface except for the formation of small clusters, and a homogeneous distribution in the bulk. As EPMA is conducted at a magnification of only 400X, it is believed that the EDS line scan has been carried out in an area depleted in Si.

It was established that *argon* had a limiting effect on the oxidation rate, decreasing the mass gain to 1.61%. Even though an inhibiting effect was identified, the Al alloy 6016 did not reach steady state for neither *synthetic air* nor *argon*, as the mass gain continued to increase even after an isothermal segment of 7 h. As previously mentioned, it was clear from the SEM images that the oxide layers were relatively equal in thickness, regardless of cover gas, and this was again confirmed by the EDS line scans analyzing a different area of the same disc sample. Figure 5d shows the elemental mapping through the line scan for the Al alloy 6016 disc sample heated in *argon*, and the same behavior was observed as for the sample heated in *synthetic air*, i.e. the concentration of oxygen first decreases, for later to increases and then decreases again from the surface through the oxide layer into the bulk. Stability diagrams from the literature [12] indicate the formation of MgO at the surface, followed by the formation $MgAl_2O_4$ before reaching the bulk where it is expected that the partial pressure of O_2 is close to zero. The EPMA confirms the behavior of Al, O, and Mg, as well as a depletion of Si at the surface, explaining why Si was not mapped by EDS.

An inhibiting effect on the oxidation rate was obtained when adding CO_2 to synthetic air in regards of mass gain, however, a thicker oxide layer was revealed when investigating the cross section by EDS, see Fig. 5f. The increase in the magnification identified the oxide layer to be around twice as thick as for the disc samples heated in *argon*, and the EDS line scan revealed a behavior more like the disc samples heated in *synthetic air*. When looking at the morphology revealed by the EDS line scan, it is observed that the oxide layer is divided into two different layers, i.e. a continuous layer on top of a layer of particles. This may be why the oxide layer is identified to be as thick, although, having a low mass gain, as the particles are only half the size of the particles identified in the oxide layer of the disc samples heated in *synthetic air*. As the density of Al (liq) is lower than the density of both MgO (liq) and $MgAl_2O_4$ (liq), it is believed that the CO_2 in the cover gas has had an inhibiting effect and thereby to some extent prevents evaporation of Mg and further oxidation, resulting in a lower mass gain of only 0.7%.

Overall Discussion

As expected, the high-Mg containing Al alloy 5182 had a higher rate of oxidation than the low-Mg containing Al alloy 6016. Due to the evaporation of Mg, and O having a higher affinity to Mg than Al, it was clear from the presently obtained results that the oxidation rate was faster when the concentration of Mg was higher. A slower oxidation rate was identified when the concentrations of Mg decreased, as steady state was not reached for the Al alloy 6016 neither when exposed to *synthetic air* nor *argon*. Even though the mass gain was 11.21% for the Al alloy 5182 and only 2.45% for the Al alloy 6016, the mass gain after 7 h in *argon* was relatively similar, i.e. 1.67% and 1.61%, respectively, indicating that the Mg concentration did not have a significant effect in an inert cover gas. An increase in the isothermal

segment may influence the mass gain, as the Al alloy 5182 disc samples reached a steady state for all cover gases in question, however, the Al alloy 6016 disc samples did not.

Diffusion of Mg towards the surface during heating was observed for all disc samples investigated in the present study, except for the Al alloy 5182 heated in CO_2 revealing a homogeneous distribution of Mg in the bulk, strengthening the theory that the Mg concentration together with the CO_2 has a significant role in obtaining an inhibition of the oxidation rate. However, as all of the Mg in the Al alloy 6016 had diffused from the bulk to the surface during heating in *synthetic air* and CO_2, and even then lowered the mass gain from 2.45 to 0.7%, it is believed that even a lower Mg concentration in combination with additions of small amounts of CO_2 in the cover gas had an inhibiting effect. Further investigations of the absorption of CO_2 on the oxide layer, e.g. MgO, is needed to evaluate how it behaves together with low- and high-Mg containing Al alloys, as it in the present study was challenging to distinguish between the C from the epoxy and the C adsorbed from the CO_2 present in the cover gas.

Conclusion

The influence of the Mg concentration and the inhibiting effect of CO_2 on the oxidation rate of aluminum has been investigated for Al alloys 5182 and 6016, by heating disc samples of the alloys to 750 °C and exposing them to three different cover gases during 7 h, i.e. (i) 80% *synthetic air* and 20% argon, (ii) 99.999% *argon*, and (iii) 76% synthetic air, 20% argon and 4% CO_2.

The present study confirmed that small additions of CO_2 to the oxidizing atmosphere had a significant inhibiting effect on the oxidation rate in the case of the high-Mg containing Al alloy 5182. The mass gain and thickness of the oxide layer decreased from 11.21% and 15–27 µm during exposer in *synthetic air* to −0.30% and 200–400 nm when additions of 4% CO_2 was added to the synthetic air. A phase transition from MgO and $MgAl_2O_4$ was identified to take place in the oxide layer inhibiting further evaporation of Mg. Mn was identified together with Al and Fe/Si as intermetallic phases in the bulk alloy, but not in the oxide layer.

A similar inhibiting effect of CO_2 was observed for the low-Mg containing Al alloy 6016, but to a lesser extent. In this case, the mass gain decreased from 2.45 to 0.7%, however, the thickness of the oxide layer itself did not decrease. A two-layered oxide deposit was identified, where the CO_2 together with the host metal had hindered further oxidation of the continuous MgO layer identified underneath the oxide layer. The Si clusters detected at the surface and the Si homogeneously distributed in the bulk alloy did not influence the oxidation rate.

Future Work

Future work includes the continuation of the analyses of the oxide layers, e.g. X-Ray Diffraction (XRD), to evaluate the phases generated as a result of exposing the disc samples to different cover gases. The isothermal segment will be increased with the aim of reaching steady state for all the cover gases in question in regard to mass gain. Moreover, different sample preparation and analysis methods will be tested to improve the mapping of C through the oxide layer.

Acknowledgements This publication has been funded by the SFI Metal Production (Centre for Research-based Innovation, 237738). The authors gratefully acknowledge the financial support from the Research Council of Norway and the partners of the SFI Metal Production.

References

1. Kos B (1995) Improvement of the metal recovery from dross by centrifuging of hot dross. In: Proceedings: Conference: 3. International Symposium on Reycling of Metals and Engineered Materials, Point Clear, AL (United States). ISBN 0-87339-318-X
2. Belitskus DL (1971) Oxidation of molten Al-Mg alloy in air, air-SO_2, and air-H_2S atmospheres. Oxid Met 3:313–317. https://doi.org/10.1007/BF00614625
3. Bergsmark E, Simensen CJ, Kofstad P (1989) The oxidation of molten aluminum. Materials Science and Engineering: A 120–121:91–95.https://doi.org/10.1016/0921-5093(89)90723-5
4. Smith N, Kvithyld A, Tranell G (2018) The Mechanism Behind the Oxidation Protection of High Mg Al Alloys with Beryllium. Metall and Materi Trans B 49:2846–2857.https://doi.org/10.1007/s11663-018-1340-6
5. Cochran CN, Belitskus DL, Kinosz DL (1977) Oxidation of aluminum-magnesium melts in air, oxygen, flue gas, and carbon dioxide. MTB 8:323–332.https://doi.org/10.1007/BF02657663
6. Surla K, Valdivieso F, Pijolat M, et al (2001) Kinetic study of the oxidation by oxygen of liquid Al–Mg 5% alloys. Solid State Ionics 143:355–365.https://doi.org/10.1016/S0167-2738(01)00861-X
7. Cochran CN, Sleppy WC (1961) Oxidation of High-Purity Aluminum and 5052 Aluminum-Magnesium Alloy at Elevated Temperatures. J Electrochem Soc 108:322–327.https://doi.org/10.1149/1.2428080
8. Do T, McIntyre NS, van der Heide PAW (1999) The oxidation kinetics of Mg-, Si- and Fe-implanted aluminum by using X-ray photoelectron spectroscopy. Surface Science 433–435:765–769. https://doi.org/10.1016/S0039-6028(99)00488-4
9. Schoenitz M, Dreizin E (2012) Oxidation Processes and Phase Changes in Metastable Al-Mg Alloys. Journal of Propulsion and Power.https://doi.org/10.2514/1.9024
10. Haginoya I, Fukusako T (1983) Oxidation of Molten Al–Mg Alloys. Trans JIM 24:613–619.https://doi.org/10.2320/matertrans1960.24.613
11. Hinton EM, Griffiths WD, Green NR (2013) Comparison of Oxide Thickness of Aluminium and the Effects of Selected Alloying Additions. MSF 765:180–184.https://doi.org/10.4028/www.scientific.net/MSF.765.180
12. Solem CKW, Ekstrøm KE, Tranell G, Aune RE (2020) Evaluation of the Effect of CO2 Cover Gas on the Rate of Oxidation of an AlMgSi Alloy. In: Tomsett A (ed) Light Metals 2020. Springer International Publishing, Cham, pp 1141–1147

13. Czerwinski F (2004) The early stage oxidation and evaporation of Mg–9%Al–1%Zn alloy. Corrosion Science 46:377–386.https://doi.org/10.1016/S0010-938X(03)00151-3
14. Smith N, Gleeson B, Saidi WA, et al (2019) Mechanism behind the Inhibiting Effect of CO2 on the Oxidation of Al–Mg Alloys. Ind Eng Chem Res 58:1434–1442. https://doi.org/10.1021/acs.iecr.8b04691
15. FactSage version 7.1 by Thermfact and GTT-Technologies